ELSEVIER

Contents lists available at ScienceDirect

Journal of Alloys and Compounds

journal homepage: www.elsevier.com/locate/jalcom



Structural and stress state dependence of small-scale deformation in bulk metallic glass



Shristy Jha, Saideep Muskeri, Siva Shankar Alla, Sundeep Mukherjee *

Department of Materials Science and Engineering, University of North Texas, Denton, TX 76203, USA

ARTICLE INFO

Article history:
Received 18 April 2023
Received in revised form 1 June 2023
Accepted 12 June 2023
Available online 15 June 2023

Keywords:
Bulk Metallic Glass
Shear Bands
Nanoindentation
Micro-Pillar Compression
Micro-Cantilever Bending

ABSTRACT

Bulk Metallic Glasses (BMGs) are attractive for myriad structural applications at multiple length scales (nano-micro-macro) but show limited bulk plasticity due to the tendency for shear localization. However, there is limited understanding of the effect of structural state and stress state on the small-scale deformation behavior of BMGs. Here, the micro-scale deformation behavior of a model Ni-based BMG was studied in as-cast and corresponding relaxed state under multiaxial nano-indentation, uniaxial micro-pillar compression, and micro-cantilever beam bending. The relaxed BMG showed 6 % higher hardness, 22 % higher yield strength, and 26 % higher bending strength compared to its as-cast counterpart. The increase in hardness, yield strength, and bending strength for the relaxed alloy compared to its as-cast counterpart demonstrates the relation of intrinsic free volume present in a BMG to its resistance for initiation of plastic events at this scale. Both the as-cast and corresponding relaxed samples showed stable notch opening and blunting during micro-cantilever bending tests rather than unstable crack propagation. However, pronounced notch weakening was observed for both the structural states, with the bending strength lower by ~ 25 % for the notched samples compared to the un-notched samples. This work may stimulate further investigations into the deformation behavior of BMGs in response to complex stress states pertinent to real-world structural applications at small scale.

© 2023 Elsevier B.V. All rights reserved.

1. Introduction

Bulk Metallic Glasses (BMGs) have attracted a lot of interest in engineering applications over the past several decades due to their excellent mechanical and surface properties, unique amorphous structure, soft magnetism, and thermoplastic processing ability [1–6]. Despite their ultra-high strength and high elastic limit, BMGs are plagued by the lack of bulk plasticity leading to catastrophic failure beyond the yield point and limiting their widespread use in structural applications. Several approaches have been utilized to mitigate the deleterious effects of shear localization in BMGs, including the introduction of secondary phases in the form of BMG composites and limiting the length-scale of BMG components to prevent catastrophic propagation of shear bands [5]. Small-scale applications of BMGs include micro/nano-electromechanical systems (MEMS/NEMS), which utilize their high strength and elasticity, potentially enabling operation over a much larger range of amplitude and frequency not achievable in state-of-the-art materials [2,3,7]. However, successful implementation in the small-scale requires fundamental understanding of failure initiation and material response to different stress states.

Fertile liquid-like regions are formed in a BMG during kinetic freezing below its glass transition temperature (T_g) , often termed as "free volume" [8–10]. When a BMG is subjected to stress beyond the yield point, plastic events are triggered to accommodate the strain and result in shear relaxation in these "free volume" regions. Collective atomic rearrangements lead to a finite shear strain, referred to as a shear transformation (ST). Successive such relaxations result in multiple STs and their interaction leads to the formation of a shear band, which accommodates the strain in a localized zone. The "free volume" model considers these STs as the carriers of plasticity. Other models, such as the Interstitialcy Theory of Condensed Matter (ITCM), consider interstitialcies (dumbbell configurations) as the basic structural defects in condensed matter and carriers of plasticity in glasses [11-13]. Other models suggest that micro-density fluctuations occur in the liquid state, which become frozen in when the temperature falls below a certain threshold (T < T_g) [14]. These fluctuations in density, which consequently cause variations in enthalpy and entropy, are referred to as "quasi-punctual defects"

Corresponding author.

E-mail address: Sundeep.Mukherjee@unt.edu (S. Mukherjee).

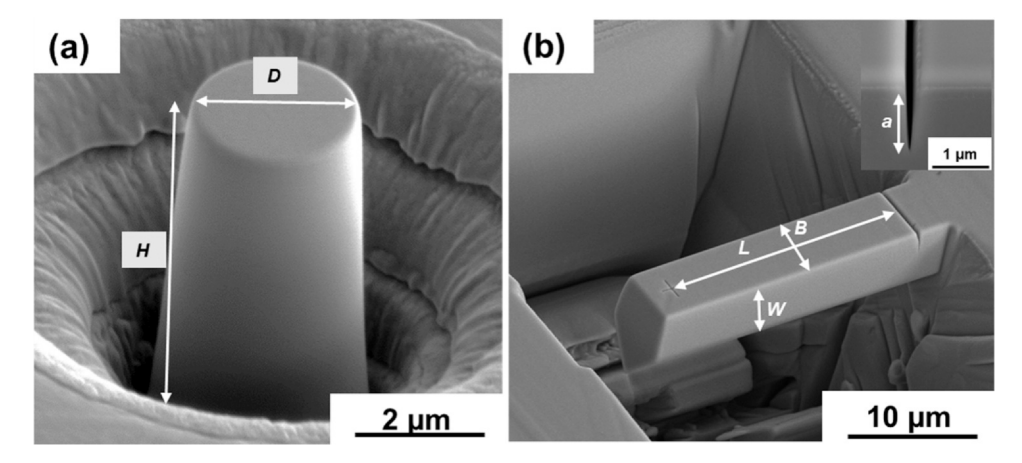


Fig. 1. (a) SEM image of a representative micro-pillar and (b) SEM image of a representative micro-cantilever with the inset image showing the notch. The symbols used for the different dimensions on the micro-pillar and micro-cantilever are marked alongside the figures.

(QPDs). This model further broadens the "free volume" concept through QPDs and includes thermodynamic frustration.

One of the factors affecting the resistance of BMGs to failure is the loading state. Under multiaxial stress field, such as indentation or bending, the resistance to failure has been reported to be better in comparison to uniaxial compression or tension due to the nature of STs and their interaction under different stress states [15,16]. However, there are few studies comparing the stress response of BMGs under different loading modes at the small-scale, where the physics of material response is unique and unconventional [1,17]. In smallscale testing, such as nano-indentation, micro-pillar compression, and micro-cantilever bending, the volume of material undergoing deformation is significantly reduced. Thus, the role of defects or heterogeneities in influencing mechanical behavior would be different and a material's intrinsic properties are often more accurately reflected in these small-scale tests. In addition to appropriate characterization of mechanical behavior for miniaturized applications, small-scale tests provide detailed insights into local stress and strain distribution that are not accessible in bulk-scale tests [18–21].

Here, the micro-scale deformation behavior of Ni₆₀Pd₂₀P₁₇B₃ bulk metallic glass (henceforth referred to as Ni-BMG) is discussed under three different loading conditions, namely multiaxial nano-indentation, uniaxial micro-pillar compression, and micro-cantilever beam bending. This alloy was chosen because Ni-based BMGs represent a model system with high strength and toughness as well as excellent glass forming ability [22-25]. The effect of structural relaxation from annealing below its T_g [26–28], was studied in each of the three deformation modes to understand the role of intrinsic free volume. As the alloy was tested at a low strain rate ($\sim 10^{-3} \text{ s}^{-1}$) and at room temperature (RT), loading response in all the cases exhibited serrated behavior [29]. Hence, these serrations were quantified concurrent with in-situ observation of deformation behavior inside a scanning electron microscope (SEM) to differentiate between the structural and stress states at the small scale. Additionally, the effect of notch in the micro-cantilever beam on the deformation behavior was investigated.

2. Experimental methods

2.1. Alloy making and structural characterization

Fully amorphous alloy with nominal composition of $Ni_{60}Pd_{20}P_{17}B_3$ was prepared in the form of a cylinder, 2 mm in diameter, by melting high purity constituents in vacuum-sealed silica tube followed by appropriate fluxing and water quenching. All the samples were metallographically prepared for x-ray diffraction

(XRD), differential scanning calorimetry (DSC), and micro-mechanical testing. DSC (NETZSCH DSC 404 C) was carried out to evaluate the characteristic temperatures and heat flow for the as-cast (AC) and heat-treated BMGs at a constant heating rate of 20 K/min. One set of samples was used in as-cast (AC) form while another set was annealed at 563 K (\sim 0.9 $T_{\rm g}$) for 20 h under argon gas environment to obtain the structurally relaxed form. Rigaku III Ultima x-ray diffractometer (Rigaku Corporation, Tokyo, Japan) with 2 mm Cu grid was used to verify the amorphous structure of both the as-cast and relaxed samples.

2.2. Mechanical behavior

Nano-indentation tests were carried out using the TI-Premier Triboindenter (Bruker, MN, USA), using a Berkovich tip, with 200 mN maximum load. A minimum of 20 indents were done on the sample with 100 µm spacing between indents to determine the hardness and modulus. For uniaxial compression, micropillars with a diameter (D) of 2.5 μ m and aspect ratio \sim 2 were milled using Ga ions at 30 keV voltage. FEI Nova NanoLab 200 focused ion beam SEM (FIB-SEM) was used with 5 nA starting current and gradually reducing to 50 pA for final finishing. The taper in the pillars was $\sim 2^{\circ}$. A representative micro-pillar is shown in Fig. 1(a). Micro-cantilevers were also milled using Ga ions with starting current of 20 nA and gradually reducing to 100 pA for the final stage. The dimensions were maintained to be 5 μ m (B) × 5 μ m (W) × 25 μ m (L), where B is the width, W is the thickness and L is the distance between the notch and the point of loading. The notch was placed at 3.5 µm from the base of the cantilever and was made using a line pattern with 10 pA current to have a small opening. The steps in reference [30] were followed to make the pentagonal cross-section micro-cantilever. A representative cantilever with all the dimensions is shown in Fig. 1(b). Both micro-pillar compression and micro-cantilever bending were carried out inside the FIB-SEM using Hysitron PI 88 Pico-indenter (Bruker, Minneapolis, MN, USA). Pillar compression was carried out with a 5 µm conical flat punch at a displacement rate of 30 nm/s. A minimum of three to five pillars were compressed on each sample to get repeatability. The engineering stress ($\sigma = F/(\frac{\pi D^2}{4})$) versus engineering strain ($\varepsilon = \Delta h/H$) was calculated from the load (F) versus displacement (h) curves (D is the pillar diameter and H is the pillar height as shown in Fig. 1(a)). The cantilevers were compressed in displacement-controlled mode using 1 µm conical flat punch at 50 nm/s using two different loading functions: (i) partial loading and unloading to 10 % of the displacement and (ii) quasistatic monotonic loading at a constant rate. For both the cases, maximum displacement was fixed at 8000 nm. Un-notched

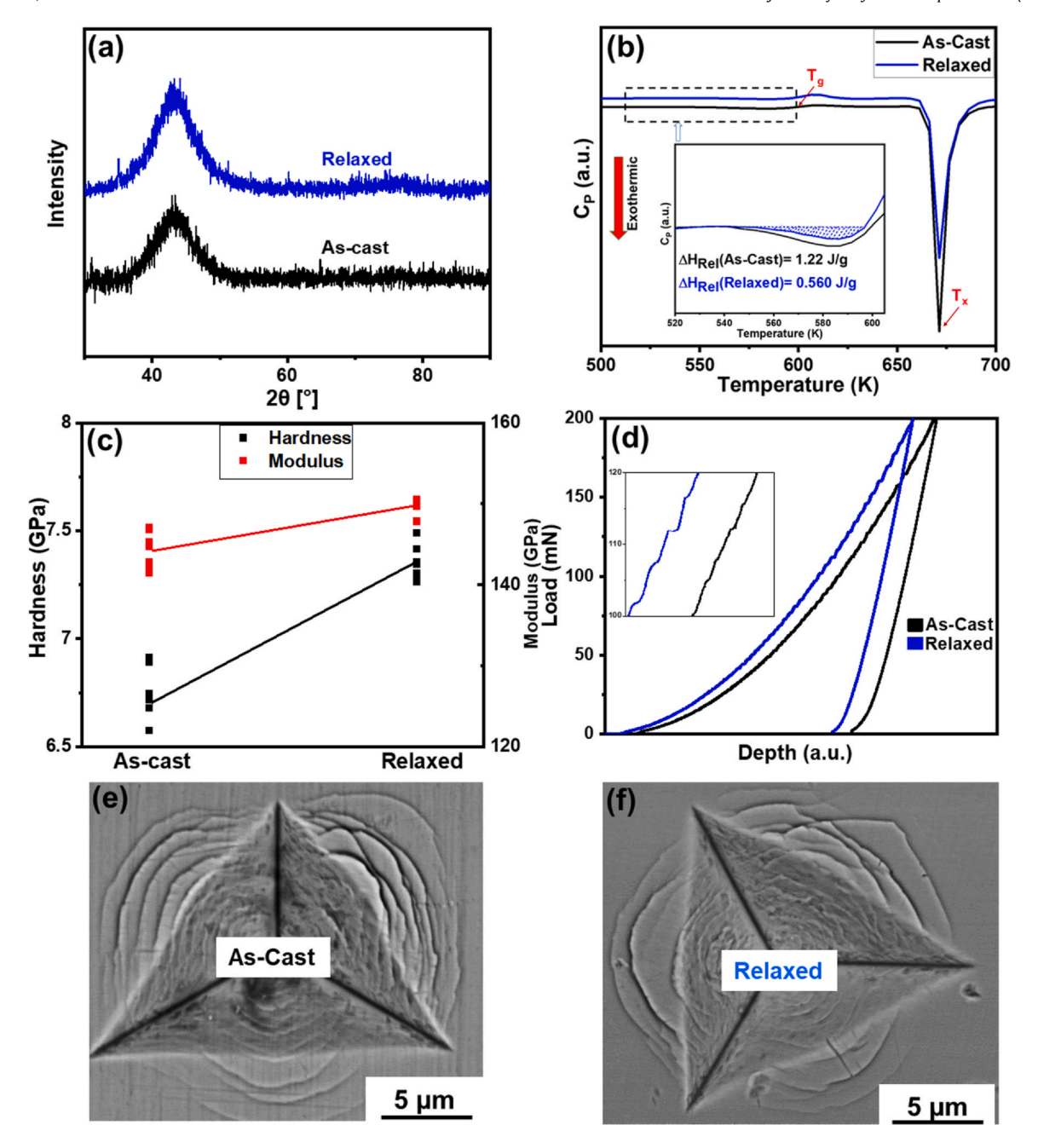


Fig. 2. (a) The amorphous nature of the as-cast and relaxed Ni-BMG confirmed by XRD; (b) Specific heat (C_p) curves obtained from DSC for the two samples, with the magnified inset image showing the area under the curves used to calculate the relaxation enthalpy (ΔH_{Rel}) prior to glass transition; (c) hardness and modulus for the as-cast and relaxed Ni-BMG obtained from nano-indentation with a trend line between the average values; (d) load versus depth plots for the as-cast and relaxed BMGs obtained at the strain rate of $4 \times 10^{-3} \text{ s}^{-1}$, with origin of the loading curves shifted by arbitrary units (a.u.) for clarity of representation; SEM image of an indent using 1 N load for: (e) as-cast Ni-BMG and (f) relaxed Ni-BMG.

cantilevers of both the samples were tested to get the bending strength values: σ_b = PLy/I; [30], where, P is the load, L is the distance between the notch and the loading point, y is the distance between the top surface of the cantilever and the neutral plane in the vertical direction, and I is the moment of inertia for the pentagonal cross-section cantilever [30]. For the notched cantilevers, because the dimensions do not satisfy the criteria given in ASTM E- 399, the conditional critical stress intensity factor (K_{OC}) was calculated as:

$$K_{QC} = \sigma_c \sqrt{\pi a} f(\frac{a}{W}) \tag{1}$$

where, σ_c is the critical bending stress determined from Eq. 3, a is the notch length, and f is a geometrical constant calculated for the pentagonal geometry as:

$$f\left(\frac{a}{W}\right) = 1.85 - 3.38\left(\frac{a}{W}\right) + 13.24\left(\frac{a}{W}\right)^2 - 23.26\left(\frac{a}{W}\right)^3 + 16.8\left(\frac{a}{W}\right)^4$$
(2)

Because precise measurement of notch extension at every loading point in the loading-unloading load function was challenging, the overall conditional J integral was measured using the following equation [31,32]. It was calculated as the sum of the elastic (J_{el}) and plastic (J_{pl}) parts:

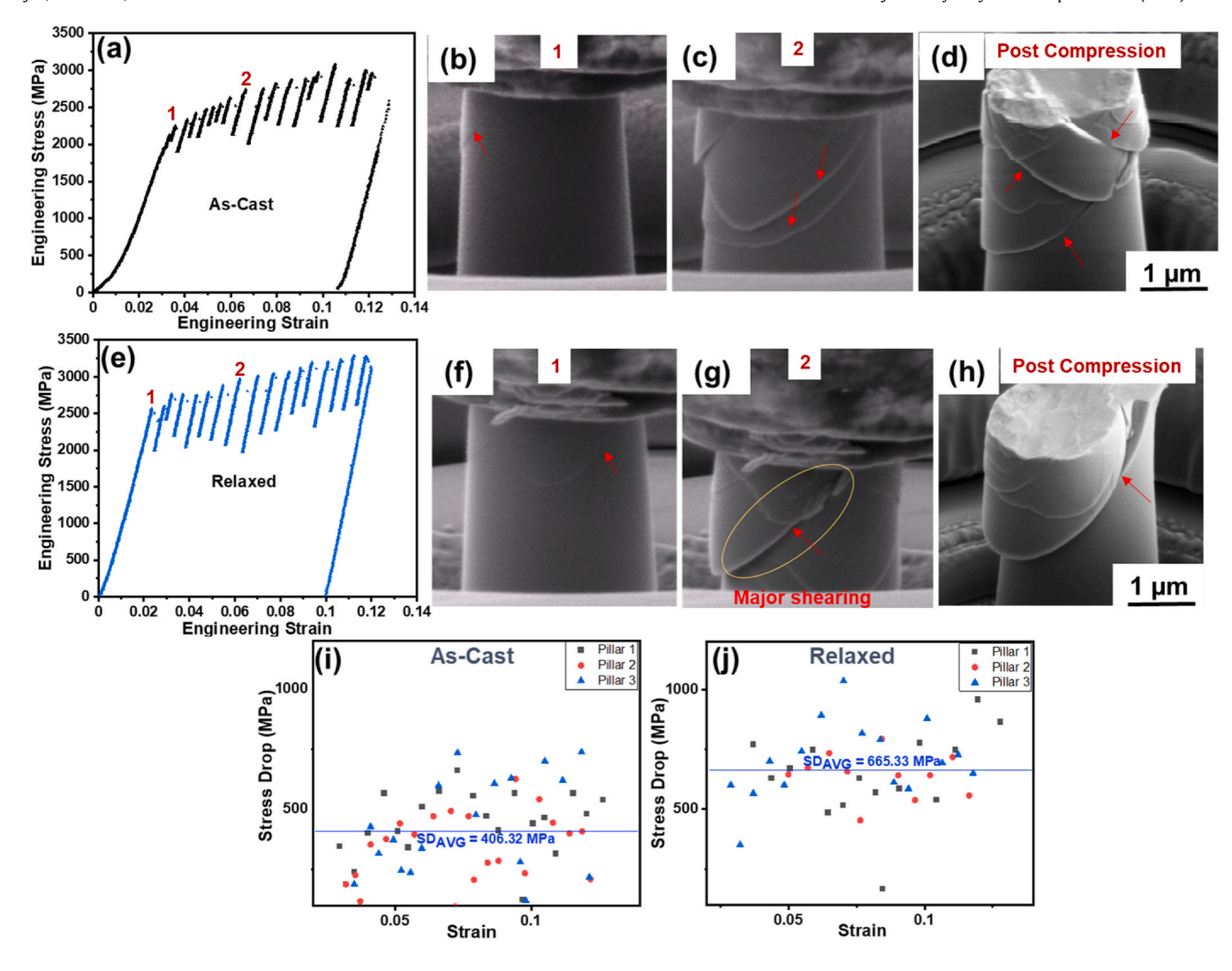


Fig. 3. Micro-pillar compression of as-cast and relaxed samples: (a) Representative engineering stress-strain curve for as-cast sample with point 1 indicating 2.5 % strain and point 2 indicating 6 % strain; In-situ video snapshot corresponding to: (b) point 1 (2.5 % strain) and (c) point 2 (6 % strain) on the stress-strain curve of the as-cast alloy with red arrows showing the shear bands; (d) Post compression secondary electron image showing the shear bands in as-cast micro-pillar; (e) Representative engineering stress-strain curve of the relaxed alloy with point 1 indicating 2.5 % strain and point 2 indicating 6 % strain; In-situ video snapshot corresponding to: (f) point 1 (2 % strain) and (g) point 2 (6 % strain) on the stress-strain curve of the relaxed alloy; (h) Post compression secondary electron image showing shear bands in the relaxed BMG pillar; (i) Load-drops for three as-cast Ni-BMG pillars as a function of strain with the average load-drop of ~ 406 MPa marked on the curve by a straight blue line; (j) Load-drops for three relaxed Ni-BMG pillars as a function of strain with the average stress drop of ~ 665 MPa marked by a straight blue line.

$$J_{C} = J_{el} + J_{pl} = \frac{(K_{QC})^{2}(1 - \nu)^{2}}{E} + \frac{\eta A_{pl}}{B(W - a) + \frac{B^{2}}{4}}$$
(3)

where, K_{QC} was calculated using Eq. (4), v is the Poisson's ratio of the material and was taken as 0.35, E is the elastic modulus that was calculated from the reduced modulus obtained from nano-indentation, η is a geometrical constant, whose value was taken as 2, A_{pl} is the area under the plastic part of the loading curve calculated using Origin Pro, while B, W and a are dimensions of the cantilever as shown in Fig. 1(b). The elastic-plastic stress intensity factor, (K_{QJ}) was calculated using the following relation:

$$K_{QJ} = \sqrt{(\frac{J_C E}{(1 - v^2)})}$$
 (4)

The diameter of the plastic zone size was estimated using the following relation:

$$D_y = \frac{1}{2\pi} (\frac{K_{QJ}}{\sigma_y})^2 \tag{5}$$

where, $\sigma_{\!y}$ is the yield strength that was calculated from micro-pillar compression.

2.3. Finite Element Analysis (FEA)

Three- dimensional (3D) elements Finite Element Analyses of notched cantilever beam were performed in ABAQUS with Mohr-Coulomb yield criterion to investigate the stress gradients on cantilever beam in displacement-controlled loading condition. A mesh was created with linear hexahedral elements of type C3D8R consisting of a total 59002 nodes and 53571 elements. A fine mesh was employed in the region close to notch tip to accurately capture the stress. A convergence mesh approach was used such that results obtained were mesh insensitive. Nonlinear analysis was conducted in this model. For fixed boundary conditions, the nodes were constrained in all the degrees of freedom. Displacement-controlled stress behavior was investigated by subjecting the micro-cantilevers to loading-unloading and monotonic loading like the experiments. Compressive yield strength and modulus values obtained from experiments were used for the simulation, while friction and dilation

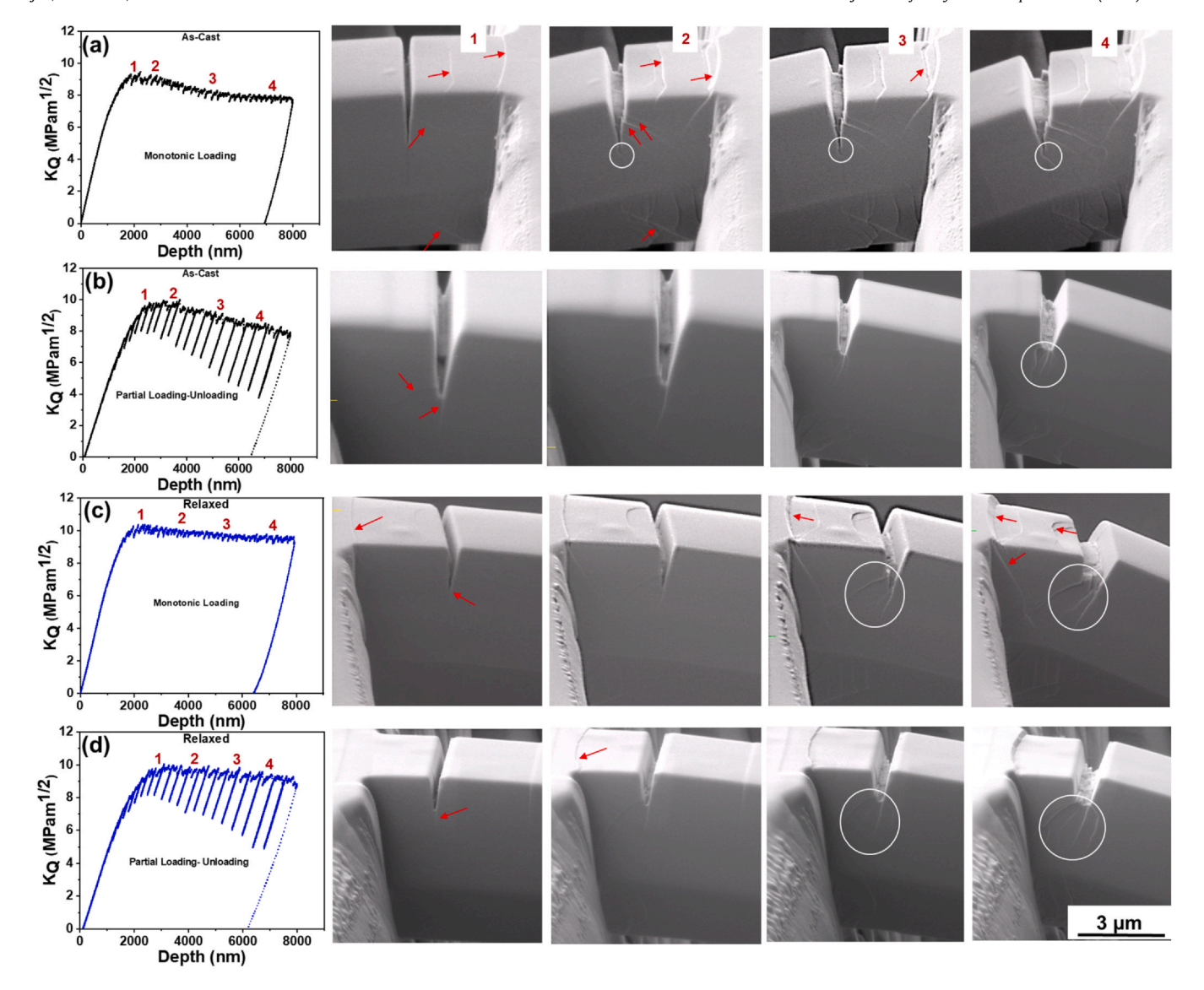


Fig. 4. K_Q versus depth curves and in-situ SEM images corresponding to displacements marked 1 through 4 on the curves for: (a) as-cast notched micro-cantilever subjected to monotonic loading, (b) as-cast notched micro-cantilever subjected to partial loading-unloading, (c) relaxed notched micro-cantilever subjected to monotonic loading, and (d) relaxed notched micro-cantilever subjected to partial loading-unloading.

angle were taken from literature on BMGs, reported as 0.15 and 0.4, respectively [33].

3. Results

3.1. Structural characterization and nanoindentation

XRD plots for the as-cast and the relaxed alloy are shown in Fig. 2(a), indicating fully amorphous structure and absence of any crystalline peaks for both the cases. Fig. 2(b) shows the specific heat (C_P) curves for the alloys measured using DSC, with the shaded region in the inset being a measure of the enthalpy of relaxation (ΔH_{Rel}) prior to glass transition. The relaxation enthalpy for the ascast alloy was measured to be 1.22 J/g while that of the relaxed alloy was less than half that value ~ 0.56 J/g, indicating significant annihilation of free volume after sub-Tg annealing. Fig. 2(c) shows the hardness and modulus data points from all the measurements corresponding to both as-cast and relaxed samples and a trend line between the average values to show the increase in both hardness and modulus for the relaxed alloy. The hardness increased from an average value of 6.7–7.1 GPa while the modulus increased from an

average value of ~ 144.6 GPa to ~ 149.8 GPa. This suggests increased stiffness of bonds from greater atomic packing after relaxation. Fig. 2(d) shows representative load versus displacement plots from nanoindentation, obtained at the strain rate of 4×10^{-3} s⁻¹, with origin of the loading curves shifted by arbitrary units (a.u.) for clarity of representation. The magnified inset image shows serrated flow behavior for both the alloys, with larger displacement bursts in case of the relaxed sample. This indicates higher resistance to shear band nucleation and relatively lower plasticity for the relaxed sample due to reduction in free volume upon annealing. Fig. 2(e) and 2 (f) show representative SEM images of indents at 1 N load for the as-cast and the relaxed samples, respectively. The density of shear bands around the indent was higher for the as-cast sample when compared with the relaxed sample. Also, the maximum deformed zone around the indent (based on an average of at least 5 measurements) was 10.6 µm for the as-cast sample compared to 9.7 µm for the relaxed sample. This indicates ~ 9 % larger deformation zone for the as-cast sample.

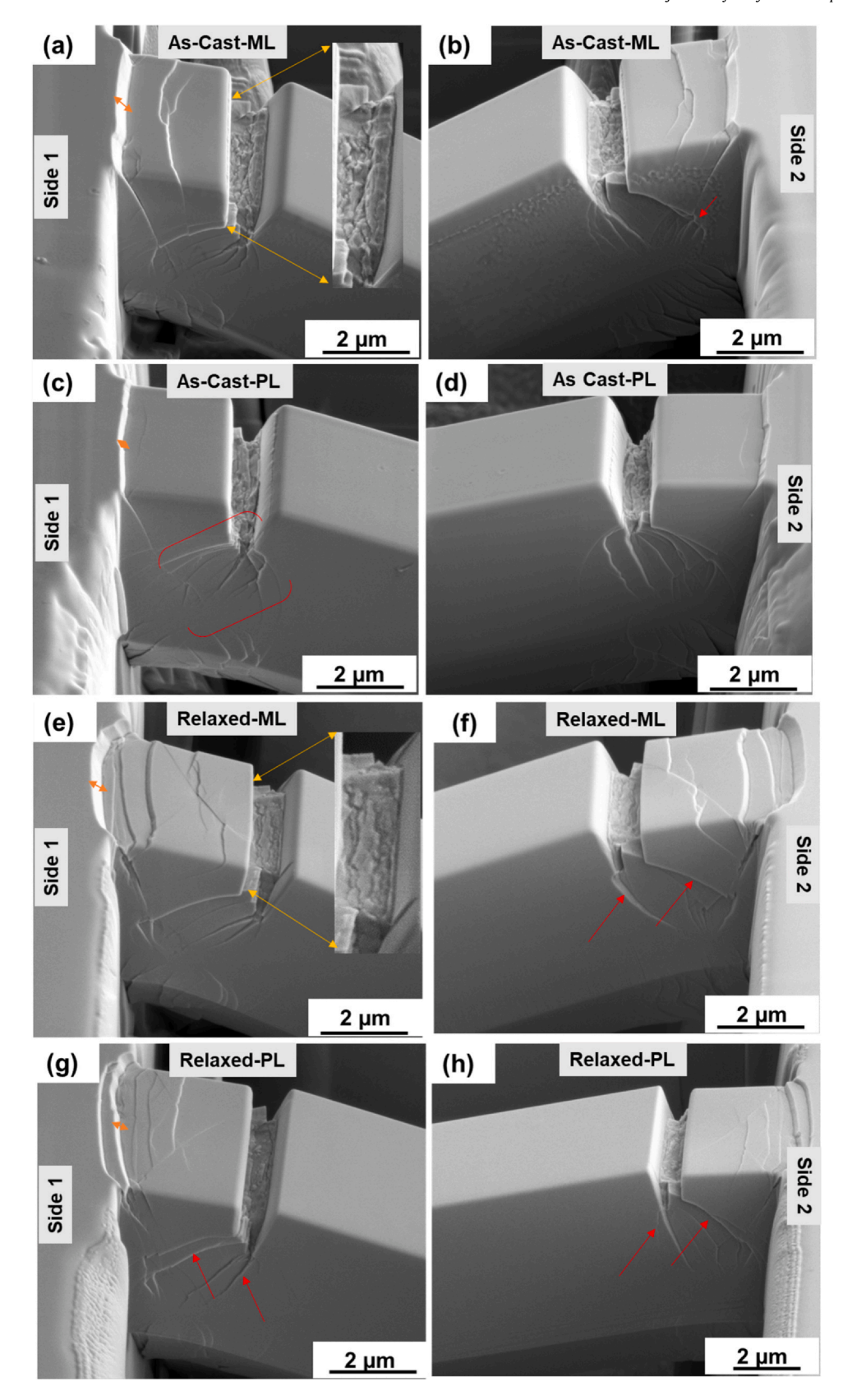


Fig. 5. Representative post-deformation SEM images showing details of shear banding around the notch for (a) as-cast micro-cantilever subjected to monotonic loading, (b) as-cast micro-cantilever subjected to partial loading-unloading, (c) relaxed micro-cantilever subjected to monotonic loading, and (d) relaxed micro-cantilever subjected to partial loading-unloading.

3.2. Micro-pillar compression

Fig. 3 shows representative micro-pillar compression results for the as-cast and relaxed samples, with the engineering stress-strain curves included in Fig. 3(a) and Fig. 3(e), respectively. Deformation behavior in both the cases is characterized by discrete serrations and stress drops, as has been reported during bulk compression of BMGs [34,35]. The yield strength (YS) was measured from the first major stress-drop during loading, which was in line with the first deformation feature observed in situ during the micro-pillar compression. The yield point is shown in the in-situ images, Fig. 3(b) and 3 (f), corresponding to position 1 on the stress-strain curves for the as-cast and relaxed sample, respectively. YS of the relaxed sample $(2.54 \pm 0.04 \, \text{GPa})$ was $\sim 22 \, \%$ higher than that of the as-cast sample $(2.07 \pm 0.119 \,\text{GPa})$. Fig. 3(c) and 3 (g) are the in-situ video shots corresponding to position 2. The stress drops were smaller in magnitude for the as-cast sample compared to the relaxed sample as shown in Fig. 3(i) and 3 (j). The average stress drop value was higher by ~ 260 MPa (64 %) for the relaxed sample compared to the as-cast counterpart, with lesser frequency and lower standard deviation.

3.3. Notched micro-cantilever bending

Fig. 4 summarizes the results for notched micro-cantilever bending of the Ni-BMG in the as-cast and relaxed states. As BMGs at this length-scale behave as semi-brittle materials [32], they typically show some plasticity near the notch prior to failure. Under these conditions, three different approaches may be used to calculate the fracture toughness via micro-cantilever bending: (i) LEFM, (ii) Rcurve behavior to calculate the I integral, and (iii) continuous stiffness measurement with EPFM analysis. In the present work, both monotonic loading (LEFM) and partial load-unload (EPFM) approaches were used to obtain the conditional fracture toughness values. Fig. 4 shows the in-situ video shots alongside the K_O versus displacement curve of a representative notched micro-cantilever for the as-cast and relaxed samples subjected to monotonic loading and partial loading-unloading. For the as-cast sample during the monotonic loading, the first shear bands appeared at the top and bottom of the cantilever as well as at the edge of the notch, as shown by arrows in Fig. 4 (a1). However, no shear bands were seen at the notch tip initially. With further compression, the initial shear bands propagated and formed steps along the notch edge at ~ 45° to the loading axis as shown by arrows in Fig. 4 (a2) and slight extension of the notch tip was seen as highlighted by a white circle. The extension propagated at an angle to the notch, leading to crack bifurcation as shown in Fig. 4 (a3 and a4). At 8000 nm final displacement, the initial shear bands formed large steps across the thickness of the cantilever base as well as near the notch but there was no catastrophic propagation of shear bands or fracture of the micro-cantilever. For the as-cast micro-cantilever subjected to partial loadingunloading, shear bands were seen at the notch edge, notch tip, and bottom of the cantilever as shown in Fig. 4 (b1-b4). But there was no sign of shear bands at the top of the base of the cantilever, unlike monotonic loading. Overall, in case of the cantilever subjected to partial loading-unloading, shear bands primarily formed around the notch-tip and bottom of the cantilever as loading progressed but there was no catastrophic failure. In case of the relaxed alloy's micro-cantilever subjected to monotonic loading, shear bands propagated to form steps at the base of the cantilever. At the notch edge, the major shear bands formed prominent steps (Fig. 4 (c1-c4)). For the relaxed micro-cantilever with partial loading-unloading, the shear bands started at the edge and the tip of the notch followed by extensive branching with increase in load (Fig. 4 (d1-d4)). Similar shear banding behavior and crack bifurcation at the notch has been reported previously for bulk notched samples of BMGs [36].

High-resolution post deformation secondary electron images of the notched micro-cantilevers from both sides are shown in Fig. 5 for different loading conditions after the final displacement of 8000 nm. In case of monotonically loaded cantilevers (Fig. 5(a), (b), (e) and (f)), large shear steps formed on the top of the cantilever, bottom edge, as well as around the notch. In contrast, for the partially loaded cantilevers (Fig. 5(c), (d), (g), (h)), shear bands formed primarily near the notch, with very few shear steps on the top or the bottom surface. In terms of difference among the two structural states, the density of primary shear bands around the notch was higher for the as-cast BMG with branched secondary shear bands (Fig. 5(a)-(d)) in contrast to fewer but more significant shear steps for the annealed BMG (Fig. 5(e)-(h)). Also, the roughness of the inner surface of the cantilever notch was different for the two structural states. As shown in the insets of Fig. 5(a) and (e), the inner surface of the as-cast BMG notch opening was rougher compared to the relaxed BMG, indicating comparatively higher energy dissipation via plastic deformation in case of the as-cast sample.

3.4. Un-notched micro-cantilever bending

To evaluate the effect of notch on bending strength, un-notched micro-cantilevers of the as-cast and relaxed BMG samples were tested as shown in Fig. 6. From the in-situ SEM snapshots, Fig. 6(a-1) and Fig. 6(b-1), shear bands started at the base of the cantilevers in both the as-cast as well as relaxed samples. With further compression, a larger number of major shear bands developed for the relaxed sample (Fig. 6(b-2)). The bending stress versus depth curves and the corresponding in-situ video snapshots are shown in Fig. 6(a) for the as-cast cantilever and Fig. 6(b) for the relaxed cantilever. The magnitude of stress drops during plastic deformation was quantified and shown in Fig. 6(c). The average stress-drop for the relaxed sample was ~ 225 MPa in contrast to a much smaller average stress-drop of ~ 85 MPa for the as-cast sample. These stress-drops correspond to nucleation of shear bands and result in the formation of shear steps on the cantilever surface. As summarized in Table 1, un-notched bending strength of the relaxed sample was ~ 26 % higher than the as-cast BMG, following similar trend in hardness and compressive vield strength between the two structural states.

4. Discussion

4.1. Small-scale deformation behavior as a function of stress state

Distinct differences in the loading response and deformation behavior were observed during nano-indentation, micro-pillar compression, and micro-cantilever bending, mainly attributed to the differences in stress state and testing geometry. Serrated behavior or "pop-ins" were observed in the *P-h* curves during nano-indentation, which has been attributed to rapid accommodation of strain by formation of discrete shear bands [37,38]. The stress-state during nano-indentation is multiaxial and geometrically constrained, with local deformation below the indent influenced by both shear and normal components. Since bulk metallic glasses do not strainharden, the plastically displaced material around the indenter tends to pile up and semi-circular pattern of shear bands are typically observed at the edge of the indent [38,39]. The shear bands shown in Fig. 2(e) and 2 (f) may be explained in terms of residual stress field around the indenter, which is circular in nature and incomplete, with lower stresses near the indent corners [38]. STs typically nucleate in regions with higher atomic disorder, larger free volume, or higher stress. The density of shear bands around the indent in ascast BMG was higher than the relaxed BMG, which may be attributed to lower free volume in the relaxed sample and structural densification from sub- T_g annealing [40]. Secondly, the relaxed alloy showed larger displacement bursts when compared to the as-cast

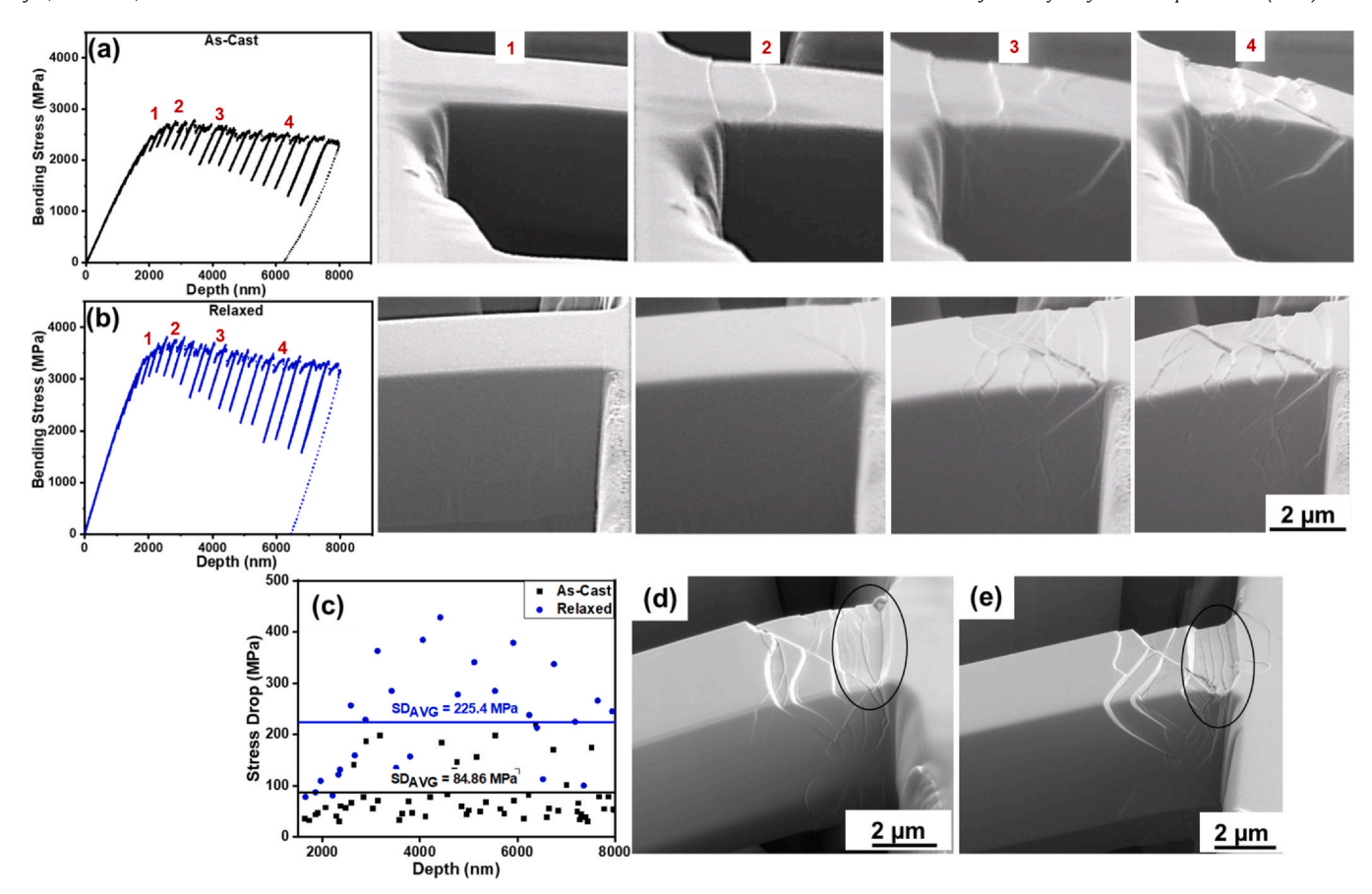


Fig. 6. Bending stress versus depth curve of a representative Ni-BMG cantilever without notch and in-situ SEM snapshots corresponding to the displacements marked 1 through 4 on the curves for (a) as-cast BMG and (b) relaxed BMG; (c) Quantification of stress drop (SD) as a function of depth for as-cast and relaxed BMGs with the average value (SD_{AVG}) for each state marked by a straight line and the value indicated alongside; Post deformation SEM image of (d) as-cast BMG cantilever and (e) relaxed BMG cantilever.

alloy, as shown in the inset of Fig. 2(d). Due to annihilation of free volume after relaxation, the energy barrier for nucleation of STs and shear band formation increases leading to bigger displacement jumps in the relaxed BMG [6]. Lower deformation resistance observed in the form of decrease in maximum shear stress was reported for a BMG after cryogenic thermal cycling due to increase in free volume [41].

In case of micro-pillar compression, the stress state is uniaxial and uniform along the length of the pillar. Due to larger free surface area, shear band propagation through the pillar thickness is easier. Shear bands initiated near the top edge and propagated as major shear bands (indicated by red arrows in Fig. 3) or via the formation of small shear steps on the micro-pillar surface, also termed as simultaneous sliding and progressive growth, respectively [42]. Loaddrops or serrations during micro-pillar compression correspond to shear band nucleation and propagation. This may be described in terms of stick-slip instability during shear banding [43,44]. In the slip part, the velocity of shear band (v_{sb}) is much higher than external loading rate (v_o), during which the elastically stored energy is released, and rapid shear band propagation occurs during the stress drop. While in the stick part, v_{sb} is less than v_o , hence the stress increases due to resistance of the material to deformation [29,45]. During micropillar compression of the relaxed BMG, larger stress

drops were observed as shown in Fig. 3(j). This suggests that the relaxed BMG has relatively higher resistance to deformation compared to the as-cast BMG, which showed smaller stress drops (Fig. 3(i)). This further manifests in terms of shear band density, with fewer shear bands for relaxed BMG (Fig. 3(h)) versus higher density of shear bands for as-cast BMG (Fig. 3(d)). This disparity may be attributed to the lower free volume of the relaxed BMG, resulting in fewer nucleation sites for STs and lower density of shear bands [6,10,40,46]. In addition, lower standard deviation in the magnitude of stress drops for the relaxed sample (Fig. 3(j)) may be attributed to the homogenization of the structure after annealing [47].

In micro-cantilever bending, there is a gradient in stress distribution with bottom part in compressive stress, top part in tensile stress, and no stress at the neutral axis. This may confine the propagation of shear bands at the neutral axis and increase in stress would lead to formation of new shear bands or activation of the existing ones [16]. This may explain the branching of shear bands near the notch along the cantilever thickness (as shown in Fig. 4 and Fig. 5) and smaller stress drops in the loading curves during microcantilever bending tests. Bending strength obtained from microcantilever test (without notch) for the as-cast sample was $\sim 35~\%$ higher than the yield strength obtained from micro-pillar compression. Similarly, the bending strength for the relaxed BMG was \sim

Table 1Hardness and Strength values of the as-cast and relaxed samples.

Samples	Hardness (GPa)	Modulus (GPa)	Compressive Yield Strength (MPa)	Un-Notch Bending Strength (MPa)	Notched Bending Strength (MPa)
As-Cast	6.7 ± 0.1	144.6 ± 1.2	2076.2 ± 119.4	2877.8 ± 173.2	2239.7 ± 459.5
Relaxed (Annealed 20 h)	7.1 ± 0.1	149.8 ± 1.3	2544.2 ± 49.6	3769.6 ± 48.8	2791.7 ± 404.5

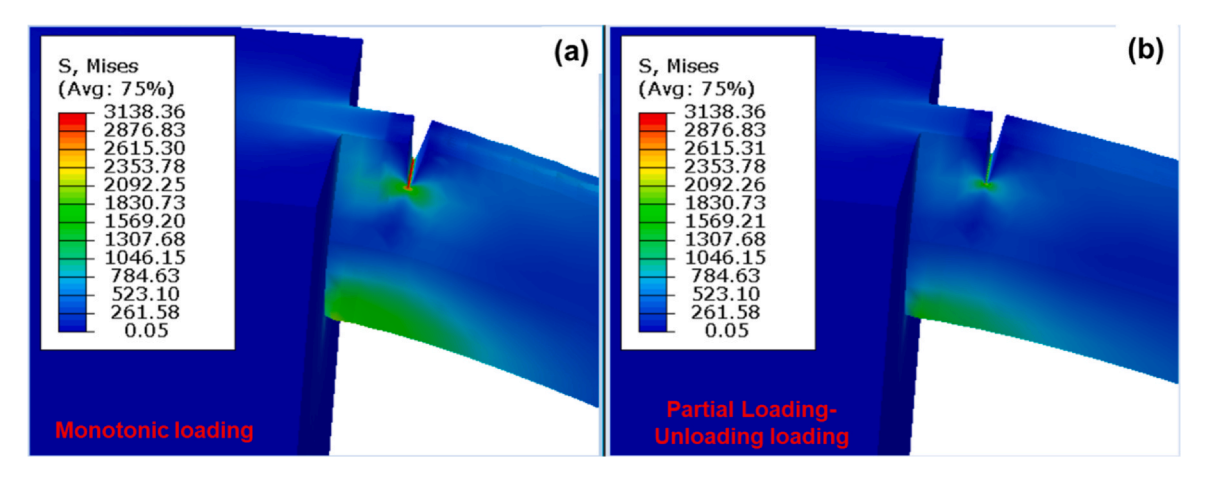


Fig. 7. FEA model for a representative micro-cantilever subjected to: (a) Monotonic loading and (b) Partial loading-unloading.

45 % higher compared to yield strength as summarized in Table 1. Confinement of shear bands due to stress gradient in micro-cantilevers leads to higher bending strength. In contrast, uniaxial compressive stress state in micro-pillars leads to lower yield strength. Unlike in compression and tension, strain hardening has been reported during bending in some BMGs because of formation and multiplication of shear bands [48].

In summary, the values of stress drop during micro-pillar compression (406 MPa for as-cast and 665 MPa for relaxed) are several times higher compared to micro-cantilever bending (85 MPa for as-cast and 225 MPa for relaxed). This indicate that uniaxial loading may be more catastrophic compared to bending at small scale for BMGs given the difference in nature of strain accommodation for these two stress states.

4.2. Micro-cantilever bending response

4.2.1. Partial loading-unloading versus monotonic loading

The stress distribution from finite element analysis of partial loading-unloading and monotonic loading of micro-cantilevers are shown in Fig. 7. The stress field in case of monotonic loading is distributed through the base and the notch of the cantilever while the stress field is more concentrated near the notch for partial loading-unloading. ASTM criteria for valid plane strain J-dominant crack field requires both B and (W-a) (ligament length, see Fig. 1(b) for the interpretation of the different symbols) to be greater than $10 \text{ J/}\sigma$, where, J is the conditional J integral calculated using Eq. 3 while σ is the yield strength calculated from pillar compression. This criterion was satisfied for the cantilevers subjected to partial loading-unloading for both as-cast as well as relaxed cantilevers, while it was not satisfied for the cantilevers subjected to monotonic loading. This may be explained by the larger strained zone for the monotonic loading case, extending even up to the cantilever base, as seen in Fig. 7(a), which leads to larger deviation from the plane strain condition. Therefore, partial loading-unloading may be the preferred mode to study shear banding behavior around the notch [49] and for satisfying the plane strain ASTM requirements. However, crack propagation was not seen for both the loading states. Deformation began with shear banding at the notch, followed by shear banding near the cantilever base, both top and bottom, along with opening of the notch and later blunting, as observed in Fig. 4. Finally, shear steps could be seen at the notch tip as illustrated in Fig. 5. At this length-scale, we see stable notch opening during bending of the cantilever, which would ultimately fail via plastic collapse rather than unstable crack propagation [37,38]. This is attributed to the fact that the critical length for shear bands to develop into cracks was not reached.

4.2.2. Un-notched versus notched bending

Throughout the BMG literature, notch weakening or strengthening seems to be unique to the system being analyzed and the length scale. Hence in the present work, one of the motivations was to quantify the bending behavior with and without notch at this length scale [50,51]. The bending strength measured for the notched cantilevers for both the as-cast and relaxed BMGs was ~ 25 % lower compared to the corresponding un-notched cantilevers. This is an indication of notch weakening, which may be attributed to the high stress concentration around the notch and stress-triaxiality that promoted the initiation of shear bands and decreased resistance to bending. Fig. 8(a) and (b) show the FEA models for stress distribution in the micro-cantilevers with notch and without notch, respectively. This may explain the observed difference in deformation via shear banding for the two cases. High stress concentration is seen around the notch for the notched cantilever (Fig. 8a) while the stress is distributed uniformly throughout the top half of the un-notched cantilever (Fig. 8(b)). For the un-notched cantilever experiment, shear bands initiated near the top base of the cantilever as shown in Fig. 6(a-2) and 6 (b-2) and the load required to nucleate these shear bands was higher. This is also apparent from the magnitude of the stress drops, which correspond to the elastic energy dissipated during shear band formation. Larger drop indicates higher energy required to nucleate a shear band. Magnified view of the bending stress curves for the un-notched and notched cantilevers obtained from experiments are shown in Fig. 8(c) and the magnitude of the corresponding stress drops are quantified as a function of depth in Fig. 8(d). Relatively larger stress drops in case of the un-notched cantilever, especially at lower depths, indicates higher energy required to activate the first shear bands and explains the prominent shear offsets seen in Fig. 6(c) and 6 (d). In contrast, a greater number of branched shear bands was seen for the notched cantilevers (Fig. 5) leading to relatively higher plasticity from the stress-triaxiality around the notch. Similar behavior has been demonstrated for macro-scale bending of Zr-based BMGs, where plastic energy accumulation due to complex stress field around the notch led to more number of shear bands and their confinement [52].

4.2.3. As-cast versus relaxed BMG

There was no catastrophic failure by crack propagation in case of both the as-cast and relaxed Ni-BMG cantilevers. The thickness of the cantilevers for all our experiments was $\sim 5~\mu m$, which is much smaller than the critical distance ($\sim 60-80~\mu m$) required to reach the critical strain proposed for BMGs [53–56]. However, the fracture surface was relatively rougher for the as-cast cantilever (shown in the inset of Fig. 5(a)) in comparison to the relaxed cantilever (shown in the inset of Fig. 5(c)). This may be explained by the micro-

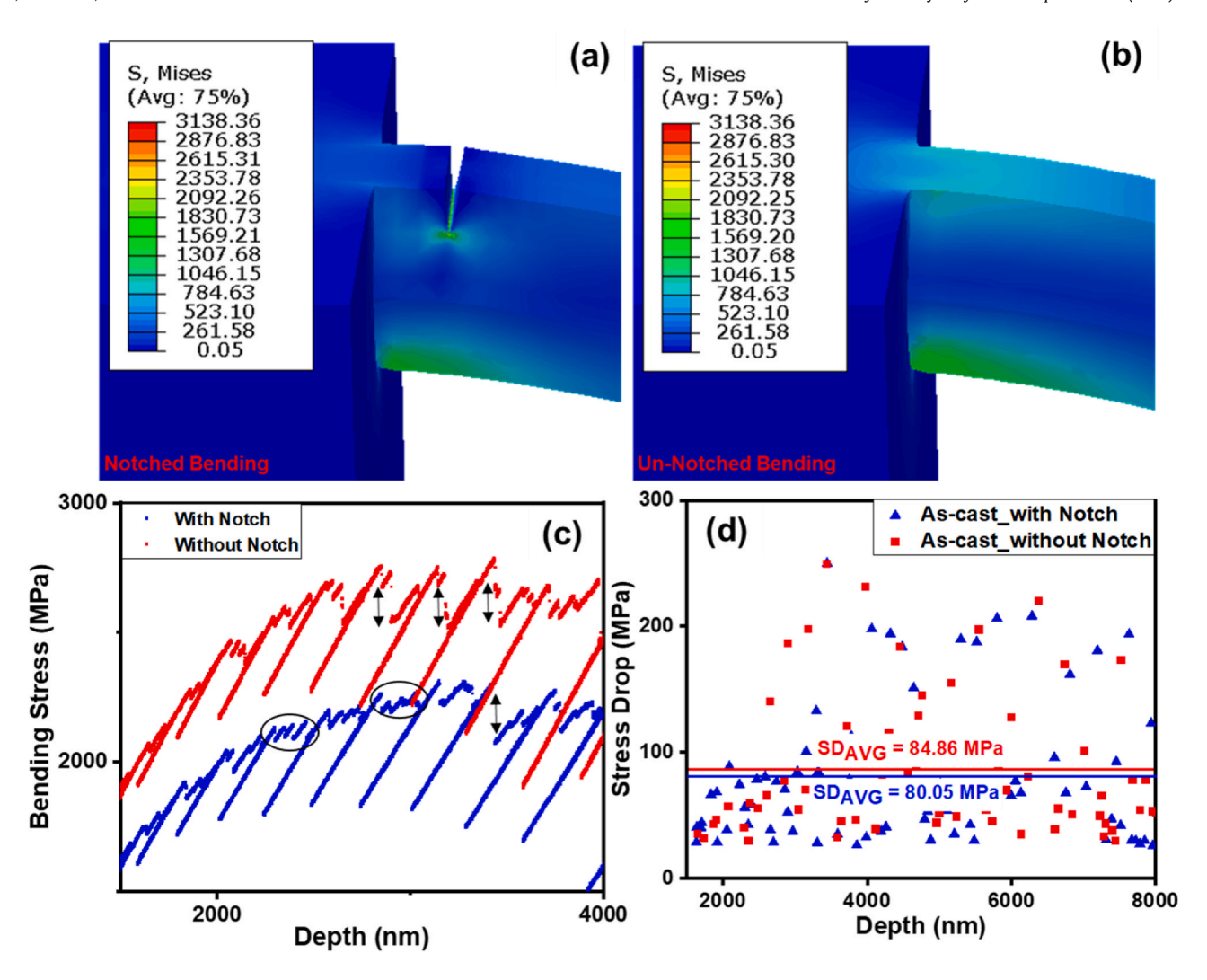


Fig. 8. FEA model showing the stress distribution for: (a) notched cantilever bending and (b) un-notched cantilever bending; (c) magnified view of the bending-stress versus depth curve showing the difference in magnitude of stress drops during un-notched and notched micro-cantilever bending experiments; (d) stress drop as a function of depth for the case of un-notched and notched micro-cantilever bending with the average stress drop (SD_{AVG}) marked by a straight line and the value indicated alongside.

mechanisms for relatively ductile BMGs proposed in the modified Argon-Salama model in terms of the fluid meniscus instability (FMI) [53,57]. Shear bands are regions of low local viscosity [58,59]. The point where shear bands nucleate ahead of the notch is referred to as the fluid meniscus, which grows under the influence of suction gradient ahead of the notch root by formation of flattened fingers with thin ligaments connected perpendicularly. After a critical strain is reached over a critical distance, the connected ligaments may rupture. This separates the initial shear band into two halves and results in ridge patterns on the fracture surface [53]. Higher the ridge heights and rougher the fracture surface, more is the crack tip opening displacement (CTOD) and higher the fracture toughness [53]. Deformation via a larger number of shear bands for the as-cast sample indicates higher plastic strain accommodated by the as-cast sample as compared to the relaxed sample. However, relatively stable behavior of the relaxed BMG observed here at the small length-scales is contrary to the brittle nature seen during bulk bending tests after sub-Tg annealing and consequent toughness reduction [26,60].

 J_c in Eq. 3 consists of two parts: (i) elastic part that depends on the strength (σ_c) and (ii) plastic part which depends on the area under the curve (A_{pl}). The plastic part for both the as-cast and relaxed Ni-BMG was small. Hence, the overall value of conditional K_{QJ} , calculated using Eq.4, was slightly higher for the relaxed sample

since its bending strength was ~ 25 % higher. Micro-cantilever bending technique may be a measure of the intrinsic fracture toughness, which is strength dominated rather than toughness controlled [61]. Also, because of the small volume of the cantilevers, both as-cast and relaxed BMGs deformed by ductile shear fracture. Multiple shear bands formed around the notch for both the cases without developing into cracks [44,62]. However, the magnitude of stress drops was larger for the relaxed sample indicating higher resistance towards ST and eventual shear band formation.

5. Conclusions

Micro-mechanical behavior of a model Ni-based BMG was investigated in as-cast and relaxed state via nano-indentation, micro-pillar compression, and micro-cantilever bending. This study sets the stage for determining the processing routes as well as loading states to design BMGs for small scale applications. The main conclusions are as follows:

i. Sub T_g annealing of the alloy led to reduction in free volume as supported by the decrease in relaxation enthalpy prior to glass transition and increase of hardness and modulus by 6 % and 5 %, respectively. The compressive yield strength (measured by micro-pillar compression) was 22 % higher and bending strength

- (measured by micro-cantilever bending) was 26 % higher for the relaxed glass compared to its as-cast counterpart.
- ii. The relaxed sample showed larger stress drops during deformation for all the three stress states indicating higher resistance towards initiation of STs. For the as-cast BMG, the stress drops were ~ 406 MPa during micropillar compression and ~ 85 MPa during microcantilever bending. The stress drops were significantly higher for the relaxed BMG, namely ~ 665 MPa during micropillar compression and ~ 225 MPa during microcantilever bending.
- iii. Semi-circular shear bands were seen around the indents after nanoindentation with higher density of shear bands and $\sim 9~\%$ larger deformation zone around the indents for the as-cast sample compared to the relaxed sample. Through-pillar failure was seen during micro-pillar compression of the relaxed sample with the propagation of major shear bands while higher density of shear bands was seen for the as-cast sample. The average magnitude of stress-drop for the as-cast BMG was $\sim 18~\%$ of its yield-strength while the average magnitude of stress-drop for the relaxed BMG was $\sim 26~\%$ of its yield-strength.
- iv. Between the two types of loading during micro-cantilever bending test, plain strain condition was satisfied for partial loading–unloading but not for monotonic loading. This was explained by the larger strained zone for the monotonic loading case, which led to larger deviation from the plane strain condition. However, failure was not seen for either case due to stable notch opening and blunting rather than unstable crack propagation. Pronounced notch weakening was observed for both the as-cast and relaxed BMGs, with the bending strength lower by ~ 25 % for the notched samples. This was attributed to the high stress concentration near the notch promoting the formation of shear bands.

CRediT authorship contribution statement

Shristy Jha.: Conceptualization, Methodology, Data curation, Writing—original draft. Saideep Muskeri.: Methodology, Visualization, Writing—review & editing. Siva Shankar Alla.: Methodology, Writing—review & editing. Sundeep Mukherjee.: Funding acquisition, Conceptualization, Supervision, Writing—review & editing.

Data Availability

Data will be made available on request.

Declaration of Competing Interest

The authors declare that they have no known competing financial interests or personal relationships that could have appeared to influence the work reported in this paper.

Acknowledgments

This work was partly supported by funding from the National Science Foundation (NSF), "USA" under grant numbers 1561886, 1919220, and 1762545. Any opinions, findings, and conclusions expressed in this paper are those of the authors and do not necessarily reflect the views of the National Science Foundation (NSF).

References

- [1] T.A. Phan, M. Hara, H. Oguchi, H. Kuwano, Current sensors using Fe-B-Nd-Nb magnetic metallic glass micro-cantilevers, Microelectron. Eng. 135 (2015) 28-31, https://doi.org/10.1016/j.mee.2015.02.043
- [2] M.F. Ashby, A.L. Greer, Metallic glasses as structural materials, Scr. Mater. 54 (2006) 321–326, https://doi.org/10.1016/j.scriptamat.2005.09.051

- [3] J. Schroers, T. Nguyen, S. O'Keeffe, A. Desai, Thermoplastic forming of bulk metallic glass—applications for MEMS and microstructure fabrication, Mater. Sci. Eng. A 449–451 (2007) 898–902, https://doi.org/10.1016/j.msea.2006.02.398
- [4] M. Chen, A brief overview of bulk metallic glasses, NPG Asia Mater. 3 (2011) 82–90, https://doi.org/10.1038/asiamat.2011.30
- [5] G. Kumar, A. Desai, J. Schroers, Bulk metallic glass: the smaller the better, Adv. Mater. 23 (2011) 461–476, https://doi.org/10.1002/adma.201002148
- [6] A.L. Greer, Y.Q. Cheng, E. Ma, Shear bands in metallic glasses, Mater. Sci. Eng. R. Rep. 74 (2013) 71–132, https://doi.org/10.1016/j.mser.2013.04.001
- [7] G.P. Zhang, Y. Liu, B. Zhang, Effect of annealing close to Tg on notch fracture toughness of Pd-based thin-film metallic glass for MEMS applications, Scr. Mater. 54 (2006) 897–901, https://doi.org/10.1016/j.scriptamat.2005.10.072
- [8] A.S. Argon, Plastic deformation in metallic glasses, Acta Met. 27 (1979) 47–58, https://doi.org/10.1016/0001-6160(79)90055-5
- [9] A.S. Argon, H.Y. Kuo, Plastic flow in a disordered bubble raft (an analog of a metallic glass), Mater. Sci. Eng. 39 (1979) 101–109, https://doi.org/10.1016/0025-5416(79)90174-5
- [10] A.S. Argon, Strain avalanches in plasticity, Philos. Mag. 93 (2013) 3795–3808, https://doi.org/10.1080/14786435.2013.798049
- [11] A.V. Granato, V.A. Khonik, An interstitialcy theory of structural relaxation and related viscous flow of glasses, Phys. Rev. Lett. 93 (2004) 155502, https://doi. org/10.1103/PhysRevLett.93.155502
- [12] A.V. Granato, The specific heat of simple liquids, J. Non Cryst. Solids 307–310 (2002) 376–386, https://doi.org/10.1016/S0022-3093(02)01498-9
- [13] A.V. Granato, Interstitialcy model for condensed matter states of face-centeredcubic metals, Phys. Rev. Lett. 68 (1992) 974–977, https://doi.org/10.1103/ PhysRevLett.68.974
- [14] J. Perez, Quasi-punctual defects in vitreous solids and liquid-glass transition, Solid State Ion. 39 (1990) 69–79, https://doi.org/10.1016/0167-2738(90)90028-P
- [15] W.F. Wu, Y. Li, C.A. Schuh, Strength, plasticity and brittleness of bulk metallic glasses under compression: statistical and geometric effects, Philos. Mag. 88 (2008) 71–89, https://doi.org/10.1080/14786430701762619
- [16] L. Zhang, F. Jiang, Y. Zhao, S. Pan, L. He, J. Sun, Shear band multiplication aided by free volume under three-point bending, J. Mater. Res. 25 (2010) 283–291, https:// doi.org/10.1557/jmr.2010.0028
- [17] B. Gludovatz, D. Granata, K.V.S. Thurston, J.F. Löffler, R.O. Ritchie, On the understanding of the effects of sample size on the variability in fracture toughness of bulk metallic glasses, Acta Mater. 126 (2017) 494–506, https://doi.org/10.1016/i.actamat.2016.12.054
- [18] R. Pippan, S. Wurster, D. Kiener, Fracture mechanics of micro samples: fundamental considerations, Mater. Des. 159 (2018) 252–267, https://doi.org/10.1016/j.matdes.2018.09.004
- [19] J. Ast, M. Ghidelli, K. Durst, M. Göken, M. Sebastiani, A.M. Korsunsky, A review of experimental approaches to fracture toughness evaluation at the micro-scale, Mater. Des. 173 (2019) 107762, https://doi.org/10.1016/j.matdes.2019.107762
- [20] V. Jayaram, Small-scale mechanical testing, Annu. Rev. Mater. Res. 52 (2022) 473–523, https://doi.org/10.1146/annurev-matsci-080819-123640
- [21] G. Dehm, B.N. Jaya, R. Raghavan, C. Kirchlechner, Overview on micro- and nanomechanical testing: new insights in interface plasticity and fracture at small length scales, Acta Mater. 142 (2018) 248–282, https://doi.org/10.1016/j.actamat. 2017.06.019
- [22] Y.Q. Zeng, J.S. Yu, Y. Tian, A. Hirata, T. Fujita, X.H. Zhang, N. Nishiyama, H. Kato, J.Q. Jiang, A. Inoue, M.W. Chen, Improving glass forming ability of off-eutectic metallic glass formers by manipulating primary crystallization reactions, Acta Mater. 200 (2020) 710–719, https://doi.org/10.1016/j.actamat.2020.09.042
- [23] J. Ketkaew, R. Yamada, H. Wang, D. Kuldinow, B.S. Schroers, W. Dmowski, T. Egami, J. Schroers, The effect of thermal cycling on the fracture toughness of metallic glasses, Acta Mater. 184 (2020) 100–108, https://doi.org/10.1016/j. acta-page 2010.10.066
- [24] L. Shao, J. Ketkaew, P. Gong, S. Zhao, S. Sohn, P. Bordeenithikasem, A. Datye, R.M.O. Mota, N. Liu, S.A. Kube, Y. Liu, W. Chen, K. Yao, S. Wu, J. Schroers, Effect of chemical composition on the fracture toughness of bulk metallic glasses, Materialia 12 (2020) 100828, https://doi.org/10.1016/j.mtla.2020.100828
- [25] J. Jeon, G. Kim, N. Seo, H. Choi, H.-J. Kim, M.-H. Lee, H.-K. Lim, S.B. Son, S.-J. Lee, Combined data-driven model for the prediction of thermal properties of Nibased amorphous alloys, J. Mater. Res. Technol. 16 (2022) 129–138, https://doi. org/10.1016/j.imrt.2021.12.003
- [26] U. Ramamurty, M.L. Lee, J. Basu, Y. Li, Embrittlement of a bulk metallic glass due to low-temperature annealing, Scr. Mater. 47 (2002) 107–111, https://doi.org/10. 1016/S1359-6462(02)00102-1
- [27] A. Slipenyuk, J. Eckert, Correlation between enthalpy change and free volume reduction during structural relaxation of Zr55Cu30Al10Ni5 metallic glass, Scr. Mater. 50 (2004) 39–44, https://doi.org/10.1016/j.scriptamat.2003.09.038
- [28] W. Dmowski, C. Fan, M.L. Morrison, P.K. Liaw, T. Egami, Structural changes in bulk metallic glass after annealing below the glass-transition temperature, Mater. Sci. Eng. A 471 (2007) 125–129, https://doi.org/10.1016/j.msea.2006.12. 137
- [29] R. Maaß, D. Klaumünzer, J.F. Löffler, Propagation dynamics of individual shear bands during inhomogeneous flow in a Zr-based bulk metallic glass, Acta Mater. 59 (2011) 3205–3213. https://doi.org/10.1016/j.actamat.2011.01.060
- [30] D. Di Maio, S.G. Roberts, Measuring fracture toughness of coatings using focused-ion-beam-machined microbeams, J. Mater. Res 20 (2005) 299–302, https://doi.org/10.1557/JMR.2005.0048
- [31] Q. Chu, Q. Cao, X. Zhu, M. Zhang, Z. Zhu, H. Zhang, R. Bai, Z. Lei, P. Cheng, C. Yan, Fracture behavior and deformation-induced structure changes of a Ti-based

- metallic glass using micro-sized cantilevers, Mater. Sci. Eng. A 833 (2022) 142519. https://doi.org/10.1016/j.msea.2021.142519
- [32] D. Sorensen, E. Hintsala, J. Stevick, J. Pischlar, B. Li, D. Kiener, J.C. Myers, H. Jin, J. Liu, D. Stauffer, A.J. Ramirez, R.O. Ritchie, Intrinsic toughness of the bulk-metallic glass Vitreloy 105 measured using micro-cantilever beams, Acta Mater. 183 (2020) 242–248, https://doi.org/10.1016/j.actamat.2019.11.021
- [33] P. Tandaiya, U. Ramamurty, G. Ravichandran, R. Narasimhan, Effect of Poisson's ratio on crack tip fields and fracture behavior of metallic glasses, Acta Mater. 56 (2008) 6077–6086.
- [34] J. Antonaglia, X. Xie, G. Schwarz, M. Wraith, J. Qiao, Y. Zhang, P.K. Liaw, J.T. Uhl, K.A. Dahmen, Tuned critical avalanche scaling in bulk metallic glasses, Sci. Rep. 4 (2014) 4382, https://doi.org/10.1038/srep04382
- [35] J. Antonaglia, W.J. Wright, X. Gu, R.R. Byer, T.C. Hufnagel, M. LeBlanc, J.T. Uhl, K.A. Dahmen, Bulk metallic glasses deform via slip avalanches, Phys. Rev. Lett. 112 (2014) 155501, https://doi.org/10.1103/PhysRevLett.112.155501
- [36] P. Lowhaphandu, J.J. Lewandowski, Fracture toughness and notched toughness of bulk amorphous alloy: Zr-Ti-Ni-Cu-Be, Scr. Mater. 38 (1998) 1811–1817.
- [37] C.A. Schuh, T.G. Nieh, A survey of instrumented indentation studies on metallic glasses, J. Mater. Res. 19 (2004) 4, https://doi.org/10.1557/jmr.2004.19.1.46
- [38] R. Vaidyanathan, M. Dao, G. Ravichandran, S. Suresh, Study of mechanical deformation in bulk metallic glass through instrumented indentation, Acta Mater. 49 (2001) 3781–3789.
- [39] C.A. Schuh, T.G. Nieh, A survey of instrumented indentation studies on metallic glasses, J. Mater. Res. 19 (2004) 4, https://doi.org/10.1557/jmr.2004.19.1.46
- [40] P. Murali, U. Ramamurty, Embrittlement of a bulk metallic glass due to sub-Tg annealing, Acta Mater. 53 (2005) 1467–1478, https://doi.org/10.1016/j.actamat. 2004.11.040
- [41] H. Zhang, Z. Wang, P.K. Liaw, J. Qiao, A criterion of the critical threshold of the maximum shear stress in bulk metallic glasses with cryogenic thermal cycling by statistics in nanoindentation, Mater. Sci. Eng. A 873 (2023) 145031, https://doi.org/10.1016/j.msea.2023.145031
- [42] H. Zhang, Z. Wang, H.J. Yang, X.H. Shi, P.K. Liaw, J.W. Qiao, A flow model in bulk metallic glasses, Scr. Mater. 222 (2023) 115047, https://doi.org/10.1016/j. scriptamat.2022.115047
- [43] B.A. Sun, S. Pauly, J. Tan, M. Stoica, W.H. Wang, U. Kühn, J. Eckert, Serrated flow and stick-slip deformation dynamics in the presence of shear-band interactions for a Zr-based metallic glass, Acta Mater. 60 (2012) 4160–4171, https://doi.org/ 10.1016/j.actamat.2012.04.013
- [44] B.A. Sun, W.H. Wang, The fracture of bulk metallic glasses, Prog. Mater. Sci. 74 (2015) 211–307, https://doi.org/10.1016/j.pmatsci.2015.05.002
- [45] R. Maa, D. Klaumünzer, G. Villard, P.M. Derlet, J.F. Löffler, Shear-band arrest and stress overshoots during inhomogeneous flow in a metallic glass, Appl. Phys. Lett. 100 (2012), https://doi.org/10.1063/1.3684871
- [46] D. Klaumünzer, A. Lazarev, R. Maaß, F.H. Dalla Torre, A. Vinogradov, J.F. Löffler, Probing shear-band initiation in metallic glasses, Phys. Rev. Lett. 107 (2011) 185502, https://doi.org/10.1103/PhysRevLett.107.185502

- [47] I.-C. Choi, Y. Zhao, Y.-J. Kim, B.-G. Yoo, J.-Y. Suh, U. Ramamurty, J. Jang, Indentation size effect and shear transformation zone size in a bulk metallic glass in two different structural states, Acta Mater. 60 (2012) 6862–6868, https://doi.org/10.1016/j.actamat.2012.08.061
- [48] Q. He, J. Xu, Locating malleable bulk metallic glasses in Zr–Ti–Cu–Al alloys with calorimetric glass transition temperature as an indicator, J. Mater. Sci. Technol. 28 (2012) 1109–1122.
- [49] D.-F. Li, C.-G. Bai, Z.-Q. Zhang, J. Zhao, Shear banding and serrated flow behaviors of high toughness Zr61Ti2Cu25Al12 bulk metallic glass under bending, Mater. Sci. Eng. A 844 (2022) 143172, https://doi.org/10.1016/j.msea.2022.143172
- [50] J. Pan, Y.X. Wang, Y. Li, Ductile fracture in notched bulk metallic glasses, Acta Mater. 136 (2017) 126–133, https://doi.org/10.1016/j.actamat.2017.06.048
- [51] R.T. Qu, M. Calin, J. Eckert, Z.F. Zhang, Metallic glasses: notch-insensitive materials, Scr. Mater. 66 (2012) 733–736, https://doi.org/10.1016/j.scriptamat.2012.01.
- [52] K. Chen, H. Wu, S.H. Chen, H.M. Zheng, Effect of complex stress fields on the plastic energy accumulation in a Zr-based bulk metallic glass, Phys. B Condens. Matter 554 (2019) 45–50, https://doi.org/10.1016/j.physb.2018.11.023
- [53] P. Tandaiya, R. Narasimhan, U. Ramamurty, On the mechanism and the length scales involved in the ductile fracture of a bulk metallic glass, Acta Mater. 61 (2013) 1558–1570, https://doi.org/10.1016/j.actamat.2012.11.033
- [54] H. Liebowitz, Fracture of Metals: An Advanced Treatise, Elsevier, 2018.
- [55] P. Tandaiya, U. Ramamurty, R. Narasimhan, Mixed mode (I and II) crack tip fields in bulk metallic glasses, J. Mech. Phys. Solids 57 (2009) 1880–1897, https://doi. org/10.1016/j.imps.2009.07.006
- [56] D. Rajpoot, P. Tandaiya, R.L. Narayan, U. Ramamurty, Size effects and failure regimes in notched micro-cantilever beam fracture, Acta Mater. 234 (2022) 118041, https://doi.org/10.1016/j.actamat.2022.118041
- [57] A.S. Argon, M. Salama, The mechanism of fracture in glassy materials capable of some inelastic deformation, Mater. Sci. Eng. 23 (1976) 219–230, https://doi.org/ 10.1016/0025-5416(76)90198-1
- [58] C.A. Schuh, T.C. Hufnagel, U. Ramamurty, Mechanical behavior of amorphous alloys, Acta Mater. 55 (2007) 4067–4109, https://doi.org/10.1016/j.actamat.2007. 01.052
- [59] J.J. Lewandowski, A.L. Greer, Temperature rise at shear bands in metallic glasses, Nat. Mater. 5 (2006) 15–18, https://doi.org/10.1038/nmat1536
- [60] Y. Huang, Z. Ning, Z. Shen, W. Liang, H. Sun, J. Sun, Bending behavior of as-cast and annealed ZrCuNiAl bulk metallic glass, J. Mater. Sci. Technol. 33 (2017) 1153–1158
- [61] R. Qu, R. Maaß, Z. Liu, D. Tönnies, L. Tian, R.O. Ritchie, Z. Zhang, C.A. Volkert, Flaw-insensitive fracture of a micrometer-sized brittle metallic glass, Acta Mater. 218 (2021) 117219, https://doi.org/10.1016/j.actamat.2021.117219
- [62] F. Jiang, M.Q. Jiang, H.F. Wang, Y.L. Zhao, L. He, J. Sun, Shear transformation zone volume determining ductile-brittle transition of bulk metallic glasses, Acta Mater. 59 (2011) 2057–2068, https://doi.org/10.1016/j.actamat.2010.12.006